Near-Infrared Fluorescent Silica/Porphyrin Hybrid Nanorings for In Vivo Cancer Imaging

Koichiro Hayashi, Michihiro Nakamura, Hirokazu Miki, Shuji Ozaki, Masahiro Abe, Toshio Matsumoto, and Kazunori Ishimura*

Ring-shaped silica nanoparticles are synthesized with a high tetrakis(4-carboxyphenyl)porphyrin (TCPP) content or silica/TCPP hybrid nanorings (HNRs) using a one-pot sol-gel reaction with a TCPP-binding silica precursor for fluorescence imaging of tumor. The shape of the HNRs is a reflection of abundant ring-shaped TCPP aggregates in the silica matrix. The HNRs are of a size that makes them susceptible to the enhanced permeability and retention effect. For comparison, the TCPP-doped silica nanoparticles are synthesized using a conventional method. The nanoparticles are spherical in shape because little TCPP is contained in the silica matrix and are designated as TCPP-containing silica nanospheres (NSs). The absorption bands of the HNRs shift by about 20 nm toward longer wavelengths compared with the TCPP bands. This redshift leads the excitation wavelength of the HNRs into the near-infrared (NIR) region. Therefore, the HNRs are excited by NIR light to emit strong fluorescence, although the NSs emit no fluorescence. The PEGylated HNRs (PEG-HNRs) are uncharged and possess a significantly longer blood circulation time than PEG-NSs. The PEG-HNRs accumulate in tumor through multiple factors including their size, uncharged surface, unique shape, and long circulation time in blood, resulting in the acquisition of clear images of tumor.

1. Introduction

Fluorescence imaging can be a useful tool for detecting tumors and tracking the distribution of cells and drugs, because it is relatively inexpensive, safe and can be performed quickly with brief exposure times. However, traditional fluorescence imaging using ultraviolet and visible light is hampered by poor tissue penetration stemming from light scattering and absorption by melanin, cytochromes, hemoglobin and water, and also a low signal-to-noise ratio due to tissue autofluorescence, which acts as background interference.[1,2] Consequently, to date, images have only been acquired at depths of a few dozen micrometers below the surface of the skin, and these images are not clear. On the other hand, fluorescence imaging in the near-infrared (NIR) region (650–900 nm) allows acquisition of deeper and clearer images in vivo because light scattering and absorption are minimal and tissue autofluorescence is diminished.[3–5] Therefore, the development of fluorescence probes with an excitation wavelength (λ_{ex}) and an emission wavelength (λ_{em}) in the NIR region is required to realize sensitive and deep tissue diagnostic imaging.

Porphyrins can be used as probes for near-infrared fluorescence imaging because their emission wavelengths (λ_{em}) are present in the NIR region, although their excitation wavelengths (λ_{ex}) are slightly shorter than NIR. It has been reported that the absorption bands of porphyrins are shifted toward longer wavelengths by enclosing porphyrins in a silica matrix.[6] In addition, porphyrins are known to form the J aggregates by π-π stacking, and this leads to the redshift of the absorption bands.[7] Furthermore, the combination of π–π stacking and electrostatic interaction yields tubular porphyrin aggregates.[8,9] Based on these findings, we have previously synthesized NIR fluorescent silica/porphyrin hybrid nanotubes using π–π stacking, electrostatic interaction and sol-gel reaction, and achieved in vivo cell tracking using the nanotubes as fluorescence probes.[10] However, the nanotubes were unsuitable as fluorescence probes for tumor imaging because they were too large in length to make use of the enhanced permeability and retention (EPR) effect, which facilitates the accumulation of nanoparticles of 50–150 nm in diameter in tumor tissue at far higher levels than in normal tissues.[11] The ring-shaped aggregates, which are the building blocks of nanotubes and are stacked to form nanotubes,[12] have the potential to achieve tumor imaging because their size is appropriate to utilize the EPR effect. In addition, high amounts of porphyrin should be included in the silica matrix to achieve clear tumor imaging and sensitive detection. Porphyrins have typically been physically entrapped inside the silica matrix by

Dr. K. Hayashi, Dr. M. Nakamura, Prof. K. Ishimura
Department of Anatomy and Cell Biology
Institute of Health Biosciences
The University of Tokushima Graduate School
3-18-15 Kuramoto-cho, Tokushima, 770-8503, Japan
E-mail: khayashi@basic.med.tokushima-u.ac.jp
Dr. H. Miki, Dr. M. Abe, Prof. T. Matsumoto
Department of Medicine and Bioregulatory Sciences
The University of Tokushima Graduate School of Medical Sciences
3-18-15 Kuramoto-cho, Tokushima, 770-8503, Japan
Dr. S. Ozaki
Department of Internal Medicine
Tokushima Prefectural Central Hospital
1-10-3 Kuramoto-cho, Tokushima, 770-0042, Japan

DOI: 10.1002/adfm.201200219

means of hydrolysis-condensation of silicon alkoxide, or the sol-gel method, in the presence of the porphyrin.[13] However, in the case of these methods, little porphyrin is contained in the silica matrix. Furthermore, the porphyrin leaks from the silica matrix resulting in low-performance imaging and side-effects. These problems can be overcome by covalent incorporation of porphyrins with silica nanoparticles, for example by means of the covalent linkage of porphyrins to mesoporous silica nanoparticles[14–16] or by the sol-gel method using porphyrin-binding silica precursors.[17,18] The porphyrin-containing mesoporous silica nanoparticles are produced by the sol-gel method using the precursors in conjunction with surfactants such as cetyltrimethylammonium bromide.[19] On the other hand, it has been reported that the molecular structures of silica precursors affect the shapes of products produced using the sol-gel method. For example, silica nanocapsules are yielded from 3-thiocyanatopropyltriethoxysilane[20] or phenyltrimethoxysilane.[21,22] Also, tetrakis(4-carboxyphenyl)porphyrin (TCPP) deposited on silica substrate forms ring-shaped aggregates.[12] Therefore, ring-shaped nanoparticles can be synthesized by means of the sol-gel reaction using a TCPP-binding silica precursor without the addition of surfactants.

In order to increase the stability of probes for in vivo fluorescence imaging, polyethylene glycol (PEG) is often introduced on to their surface, a process known as PEGylation. PEGylation often masks the probes from the host's immune system, reducing antigenicity and immunogenicity.[23] In addition, PEGylation can prolong the circulatory time of probes by reducing renal clearance, and can decrease the toxicity of the probes and render them water soluble.

In the present study, we have demonstrated that ring-shaped silica nanoparticles with a high TCPP content, or silica/TCPP hybrid nanorings (HNRs), can be synthesized by means of the one-pot sol-gel reaction using a TCPP-binding silica precursor. The λ_{em} and λ_{ex} of the HNRs were in the NIR region and were of a size that made them susceptible to the EPR effect. Furthermore, using the PEG-modified HNRs (PEG-HNRs) as a probe, we accomplished clear imaging and sensitive detection of tumor by NIR fluorescence imaging.

2. Results and Discussion

2.1. Synthesis and Characterization

The TCPP-binding silica precursor was prepared by amidation between TCPP and 3-aminopropyltriethoxysilane (APTES) (**Scheme 1**A). The silica/TCPP HNRs were synthesized by

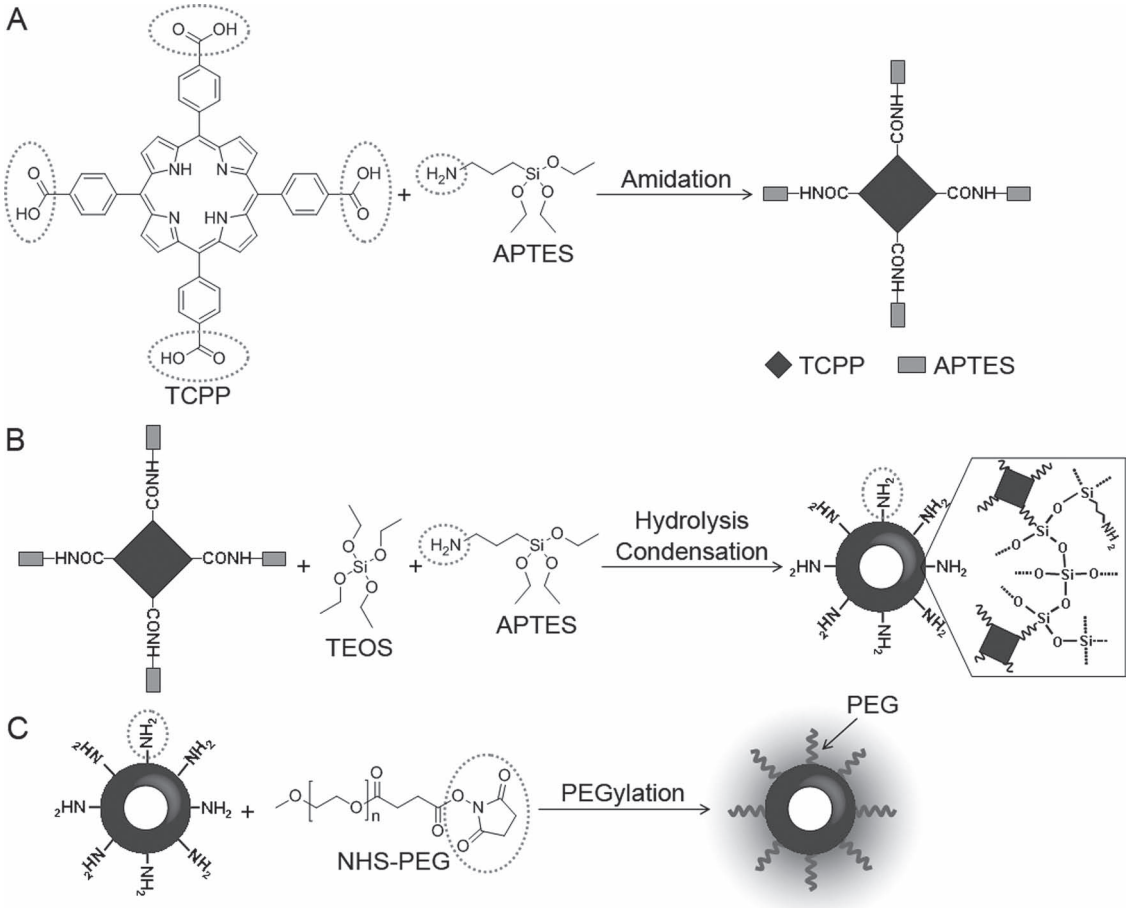

Scheme 1. A) Preparation of TCPP-binding silica precursor via the amidation reaction between TCPP and APTES. B) Synthesis of silica/TCPP HNRs by means of the sol-gel reaction using TCPP-binding silica precursor, TEOS, and APTES. C) PEGylation of silica/TCPP HNRs via amidation reaction.

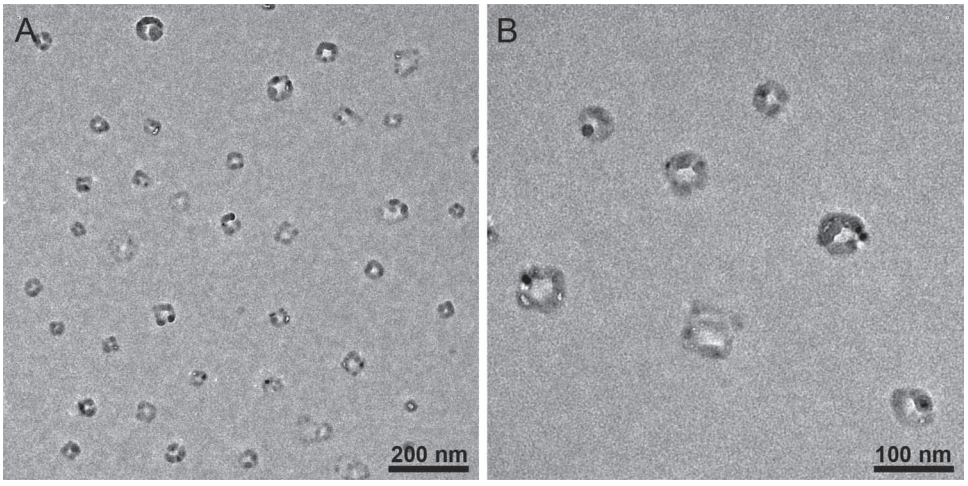

Figure 1. TEM images of silica/TCPP HNRs.

means of the sol-gel reaction using the precursor, tetraethyl orthosilicate (TEOS) and APTES, which provided the amino groups on the surface of the HNRs for subsequent PEGylation (Scheme 1B). PEGylation was easily achieved due to the reaction between the amino groups on the surface of the HNRs and *N*-hydroxysuccinimide (NHS) activated PEG ester groups (Scheme 1C). For comparison, physical TCPP-containing silica nanospheres (NSs) were synthesized by means of the sol-gel reaction using TEOS and APTES in TCPP solution.

The shape and size of the silica/TCPP HNRs and the TCPP-containing silica NSs were observed using transmission electron microscopy (TEM). The HNRs were ring-shaped particles with a diameter of 56 nm ± 9 nm (**Figure 1**A,B). The shape of the HNRs was a reflection of abundant ring-shaped TCPP aggregates in the silica matrix.[7] On the other hand, the NSs were solid spherical particles with a diameter of about 243 nm (Supporting Information Figure S1A,B) because they contained little TCPP.

The structure of the HNRs was analyzed using Fourier transform infrared spectroscopy (FTIR) and solid-state nuclear magnetic resonance (NMR), as shown in **Figure 2**. The absorption bands at 1160 – 1050 cm^{-1} were due to ν Si–OR in the FTIR spectra of TEOS and APTES (Figure 2A).[24] The band attributed to δ N–H of amine was also present at 1584 cm^{-1} in the spectrum for APTES.[25] In the spectrum for TCPP, the band at 1410 cm^{-1} was assigned to ν $C_\alpha N$, ν $C_\alpha C_\beta$ and the bands at 1780 – 1650 cm^{-1} were due to ν C = O in carboxylic acid.[26] In the spectrum for the HNRs, the bands at 1069 cm^{-1}, 806 cm^{-1} and 473 cm^{-1} were due to ν_{as} Si–O–Si, ν_s Si–O–Si and ρ Si–O–Si, respectively.[25,27,28] The band attributed to the amide ν C = O was observed at 1650 cm^{-1}, whereas the band due to the carboxylic acid ν C = O was not present. The band at 1554 cm^{-1} was ascribable to the δ N–H of the amide and amine. The band due to the TCPP ν $C_\alpha N$ and ν $C_\alpha C_\beta$ was also present at 1395 cm^{-1}. These results revealed that a siloxane network was formed by the sol-gel reaction of silica precursors, and TCPP was included in the siloxane network due to the amide linkage. The structure of the HNRs was analyzed in more detail using solid-state ^{29}Si- and ^{13}C-NMR (Figure 2B and 2C). In the ^{29}Si cross-polarization (CP)/magic angle spinning (MAS) NMR spectrum (Figure 2B), three resonance peaks at –108.0 ppm, –100.4 ppm and –66.7 ppm were due to the Si environments of Q^4, Q^3 and T^3, respectively.[25,28] The peak at –66.7 ppm had a shoulder, which was assigned to the T^2 unit. These results established that the three or four alkoxy groups of TEOS, and the two or three alkoxy groups of TCPP-binding silica precursor and APTES, underwent a hydrolysis and condensation reaction to form a siloxane network in the HNRs. In the ^{13}C CP/MAS NMR spectrum (Figure 2C), peak 1 at 10.4 ppm and the peak 2 at 22.3 ppm were assigned to the C^1 and C^2 of the $SiC^1H_2C^2H_2C^3H_2NHR$ (R = C or H), respectively.[25] Peak 3 at 35.4 ppm and peak 11 at 42.7 ppm were attributed to C^3 bound to amide and amine, respectively. Peaks 5–10 at 110–155 ppm were due to TCPP.[29] Peak 4 was assigned to the amide formed by condensation between the carboxylic acid of TCPP and the amine of APTES. Peak 12 was due to the carboxylic acid of TCPP. These results demonstrated that TCPP was incorporated into the siloxane network at the molecular level via amide linkage, and furthermore, that HNRs were functionalized with amino groups that were useful for PEGylation.

The contents of TCPP in the HNRs and the NSs were estimated from their weight losses determined by thermogravimetric (TG) analysis (**Figure 3**). The total weight losses of the HNRs and the NSs were 58 wt% and 13 wt%, respectively. A proportion of this weight loss due to evaporation of adsorbed water was about 13 wt% and 8 wt% for the HNRs and the NSs, respectively. Thus, the organic phase incorporated in the HNRs and the NSs, which was mainly TCPP, was 45 wt% and 5 wt%, respectively. Based on these values, the contents of TCPP in the HNRs and the NSs were approximately 570 μmol/g and 63 μmol/g, respectively. These findings indicated that the sol-gel method using TCPP-binding silica precursor was significantly more effective at increasing the TCPP content in the siloxane network than physical trapping of TCPP in the siloxane network.

2.2. Optical and Fluorescent Properties

The HNRs-dispersed saline appeared reddish brown due to abundant TCPP incorporated in the siloxane network

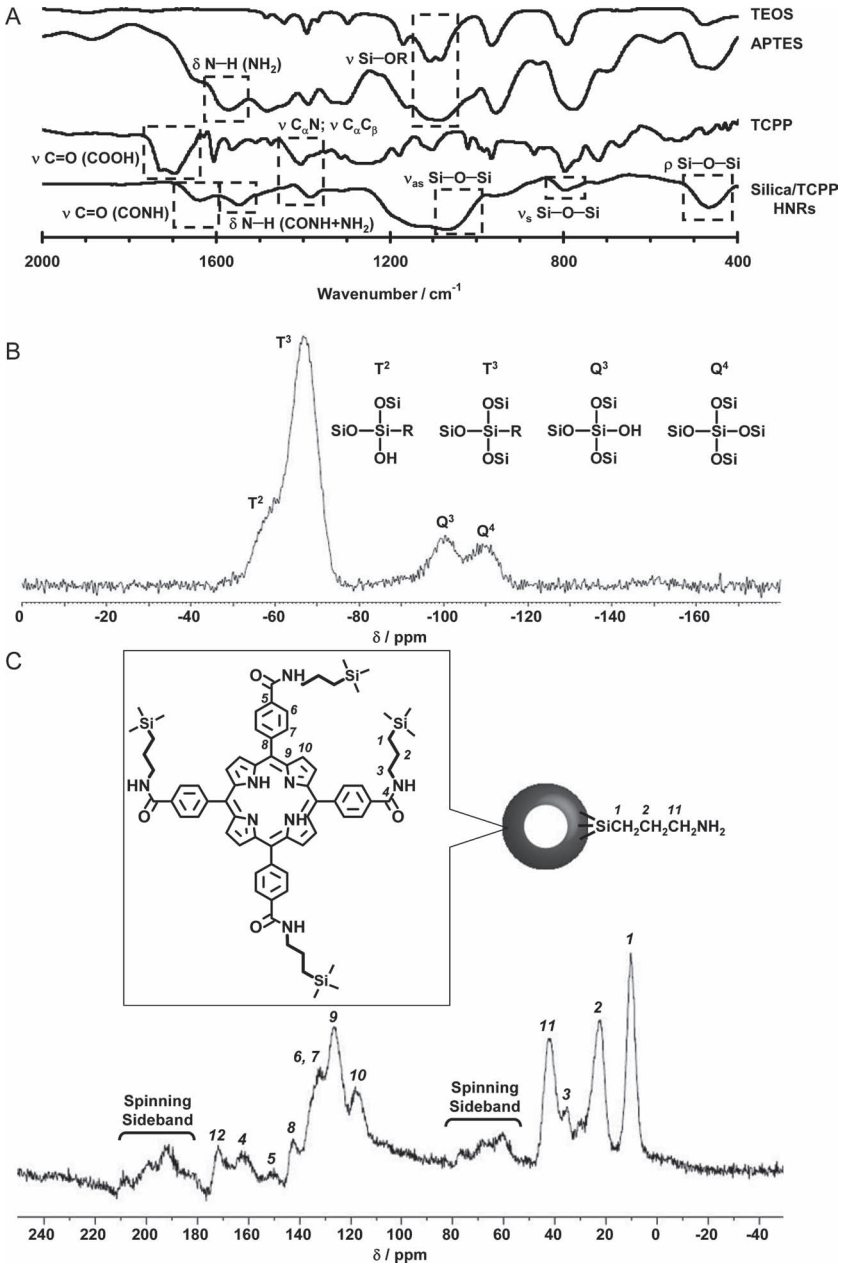

Figure 2. A) FTIR spectra of TEOS, APTES, TCPP and silica/TCPP HNRs. B) Solid state ^{29}Si CP/MAS NMR spectrum of silica/TCPP HNRs. C) Solid state ^{13}C CP/MAS NMR spectrum of silica/TCPP HNRs.

(Supporting Information Figure S2A). On the other hand, the NSs-dispersed saline appeared white, which was a pure silica color, because the NSs contained limited amounts of TCPP (Supporting Information Figure S2B). For the same reason, the absorption bands attributed to TCPP were confirmed in the absorption spectrum of the HNRs, whereas they were not found in the spectrum of the NSs (**Figure 4**). Furthermore, the absorption bands of the HNRs shifted by about 20 nm toward longer wavelengths in saline as compared with the TCPP bands. This redshift was caused by both enclosing TCPP in a silica matrix[6] and formation of ring-shaped aggregates, J-aggregates, via π-π stacking[7–11] and led the maximum wavelength of the absorption band, λ_{ex}, of the HNRs into the NIR region, resulting in acquisition of deeper and clearer images.

The fluorescence images indicated that the HNRs were excited by NIR light (λ_{ex} = 675 nm) to yield the NIR fluorescence (λ_{em} > 720 nm) in the saline as shown in Supporting Information Figure S3, whereas the NSs emitted no fluorescence (Supporting Information Figure S4). Furthermore, the average radiant efficiency (RE) of the HNRs was maximal at 720 – 740 nm and was decreased with increasing wavelength (**Figure 5**A). The max RE of the HNRs reached a maximum at 740 nm (Figure 5B). Thus, the optimum λ_{ex} and λ_{em} of HNRs were 675 nm and 740 nm, respectively.

2.3. PEGylation

PEGylation of the HNRs was confirmed using FTIR spectra (**Figure 6**A). In the spectrum of NHS activated ester groups-functionalized PEG (NHS-PEG), the band attributed to the ν C = O of NHS activated ester was present at 1744 cm^{-1}.[30] On the other hand, this band disappeared in the spectrum for the HNRs and the bands assigned to ν C = O and δ N–H of the amide appeared at 1666 cm^{-1} and 1554 cm^{-1}, respectively.[30] Furthermore, the bands derived from PEG were observed at 965 cm^{-1} and 560 cm^{-1}.[30] The bands due to ν_{as} Si–O–Si, ν_s Si–O–Si and ρ Si–O–Si of the siloxane linkage were present at 1072 cm^{-1}, 802 cm^{-1} and 455 cm^{-1}, respectively.[25,27,28] These results confirmed that PEGylation of the HNRs was achieved by the amidation of the amino groups of the HNRs and the NHS activated ester groups of NHS-PEG.

The hydrodynamic diameter of the HNRs was 60 ± 24 nm in saline measured by dynamic light scattering (DLS) as shown in Figure 6B, which was consistent with the TEM result. After PEGylation, the hydrodynamic diameter increased to 98 ± 37 nm. These findings indicated that PEGylation of the HNRs was achieved.

The zeta potential of the HNRs in saline changed from –11.6 mV to +0.45 mV by PEGylation (Figure 6C). Thus, the surface charge of the PEG-HNRs was almost zero. This finding suggested that the PEG-HNRs were less subjected to adhesion of various biomolecules such as protein and could circulate in blood for long period time.

The amount of PEG linked to the HNRs was estimated from the weight loss measured using TG. The total weight losses of the PEG-HNRs was 71 wt% determined using TG curves (Supporting Information Figure S5). A proportion of this weight loss

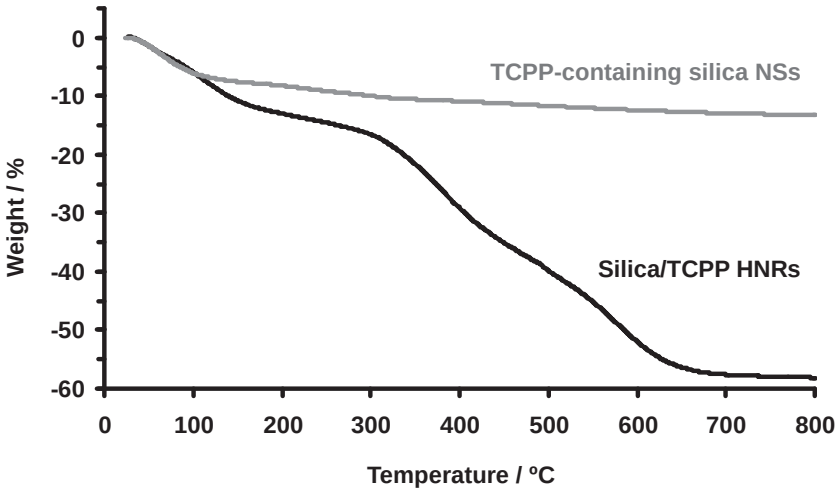

Figure 3. TG curves of silica/TCPP HNRs (black) and TCPP-containing silica NSs (gray).

due to evaporation of adsorbed water was about 18 wt% for the PEG-HNR. Thus, the organic phase incorporated in the PEG-HNRs was 53 wt%. Because the organic phase incorporated in the HNRs before PEGylation was 45 wt% as shown in Figure 3, the proportion of PEG linked to the HNRs was estimated to be 8 wt%. Based on this value, the amount of PEG linked to the HNRs was approximately 40 μmol/g. Maldiney et al. have determined the amount of PEG (5 kDa) covering nanoparticles by the same method as ours and have reported that it was 15 μmol/g.[31] Considering the molar weight of PEG, our result is consistent with that by obtained Maldiney et al.

2.4. Tumor Imaging

We injected the PEG-HNRs intravenously into tumor-bearing mice and investigated their biodistribution using NIR fluorescence imaging (λ_{ex} = 675 nm and λ_{em} = 740 nm). Tumor with a yellow circle was clearly detected in vivo. Both the total RE and max RE of the tumor were increased over a 6 h period after injection, remained stable until 12 h, and subsequently declined (**Figure 7**A,B). Thus, the PEG-HNRs progressively accumulated in the tumor over the first 6 h after injection, remained at a constant level for a further 6 h, and then gradually migrated from the tumor and dispersed throughout the body. Renoir et al. have reported the RPMI 8226 tumor, myeloma, was richly vascularized and their vasculature endothelium was discontinuous.[32–34] Furthermore, they demonstrated that liposomes with a diameter of 150 nm were useful as drug carriers for myeloma. This finding suggests that the fenestration size of the endothelium is estimated to be 150 nm at least. The hydrodynamic diameter of the PEG-HNRs was about 100 nm and was less than the fenestration size of the endothelium. Therefore, the PEG-HNRs highly accumulated in the tumor. Additionally, we investigated the biodistribution of the PEG-HNRs 6 h after injection when the PEG-HNRs accumulated in the tumor at the highest level. Supporting Information Figure S6 shows the dorsal, lateral and ventral fluorescence images of tumor-bearing mouse before and after injection. The PEG-HNRs appeared to accumulate in the tumor locally in the dorsal images (Supporting Information Figure S6A). However, the lateral and ventral images indicated that the PEG-HNRs were located not only in the tumor but also in a site other than tumor (Supporting Information Figure S6B,C), which was identified as the small bowel by the dissected image (Supporting Information Figure S6D). Because the small bowel accounts for about half of all blood capillary throughout the body, the fluorescence signals were probably observed there. Whereas nanoparticles generally accumulate in the liver and spleen because of reticuloendothelial system (RES) uptake, no fluorescence signal emitted from the PEG-HNRs was found in these organs. Although this reason is not known exactly so far, not only the effect of PEGylation but also the uncharged surface and the unique shape of the PEG-HNRs may contribute to escape RES uptake based on the reports by Mitragotri et al., which revealed that the charge and the shape of nanoparticles are crucial parameters that affect avoidance of phagocytosis by macrophages.[35–40] The ex vivo imaging of tumor-bearing mouse injected with the PEG-HNRs also established that they locally accumulated not in liver and spleen but in the tumor (Figure 7C). Furthermore, we investigated the blood circulation time by selecting six 2 mm × 2 mm regions of interest (ROI) per mouse, where these ROI were selected to accord with conspicuous surface blood vessels, and by tracking them through time. Mean RE values from six ROI on each mouse were measured and plotted versus time after injection as shown in Supporting Information Figure S7. The half-life ($t_{1/2}$) of the PEG-HNRs in blood was about 5.5 hours. He et al. have measured the $t_{1/2}$ of PEG-modified silica NSs (PEG-NSs) by the same method as ours and reported that it was about

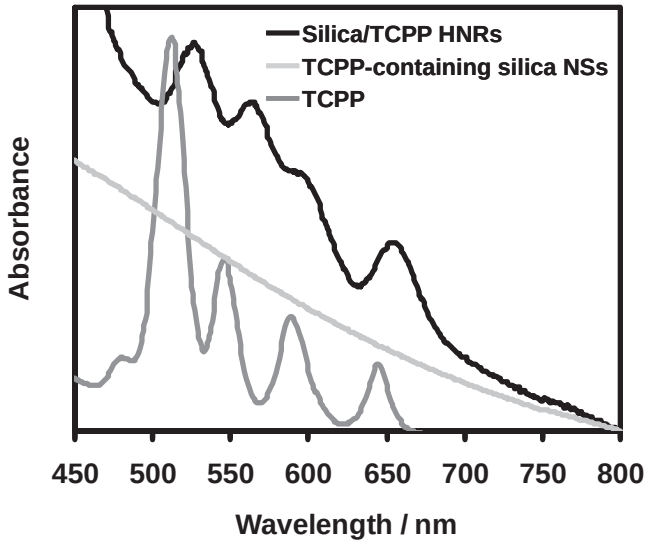

Figure 4. Absorption spectra of TCPP, silica/TCPP HNRs, and TCPP-containing silica NSs in saline.

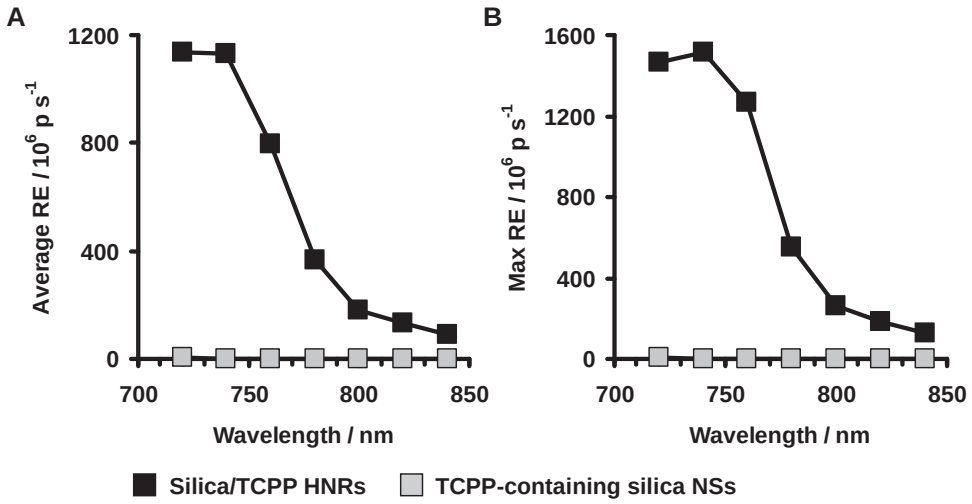

Figure 5. A) Average RE and B) max RE of silica/TCPP HNRs (black) and TCPP-containing silica NSs (gray) in saline.

3 hours.[41] Thus, the PEG-HNRs possessed a significantly longer $t_{1/2}$ than the PEG-NSs, which indicated that fewer PEG-HNRs were taken up by RES compared to the PEG-NSs. Above results demonstrated that the PEG-HNRs highly accumulated in tumor because of multiple factors such as their size, charge, shape and blood circulation time, resulting in acquirement of clear image of tumor. Therefore, the PEG-HNRs can function as a probe for use in NIR fluorescence imaging of tumor.

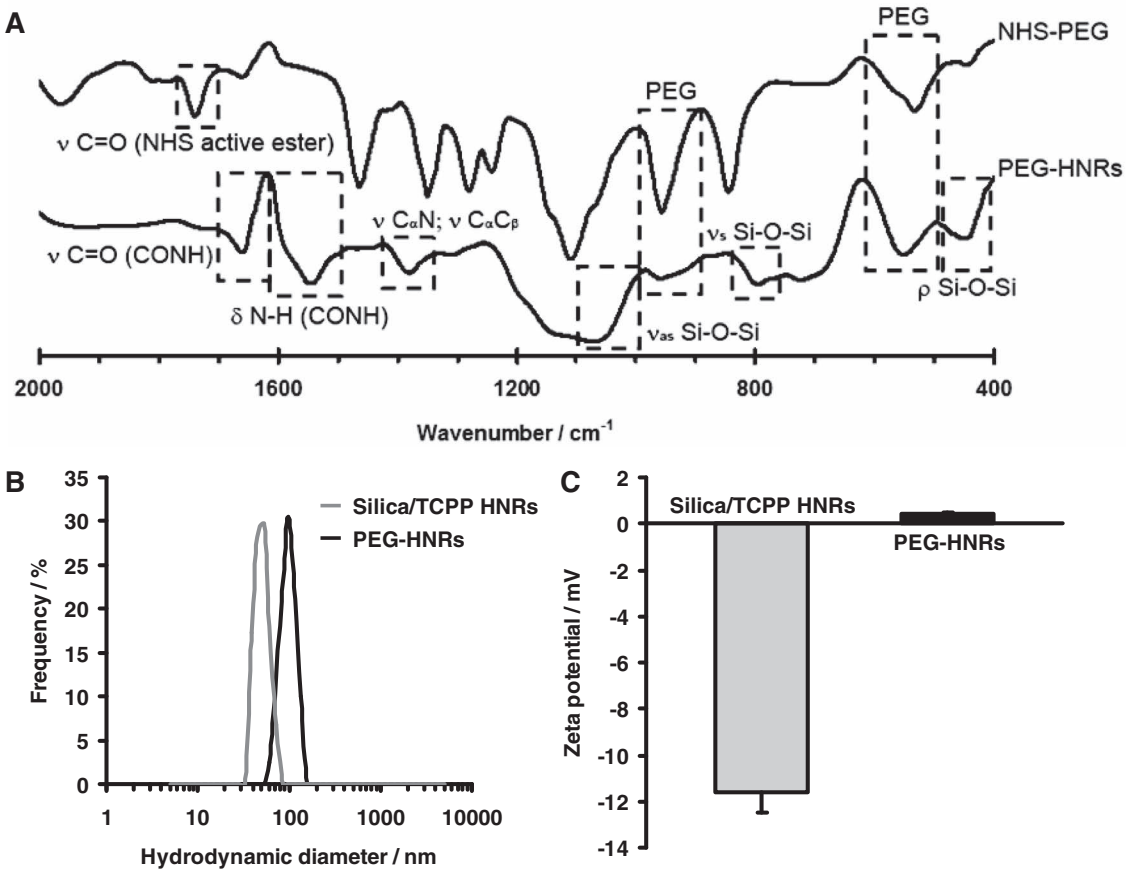

Figure 6. A) FTIR spectra of NHS-PEG and PEG-HNRs. B) DLS curves of silica/TCPP HNRs and PEG-HNRs in saline. C) Zeta potentials of silica/TCPP HNRs and PEG-HNRs.

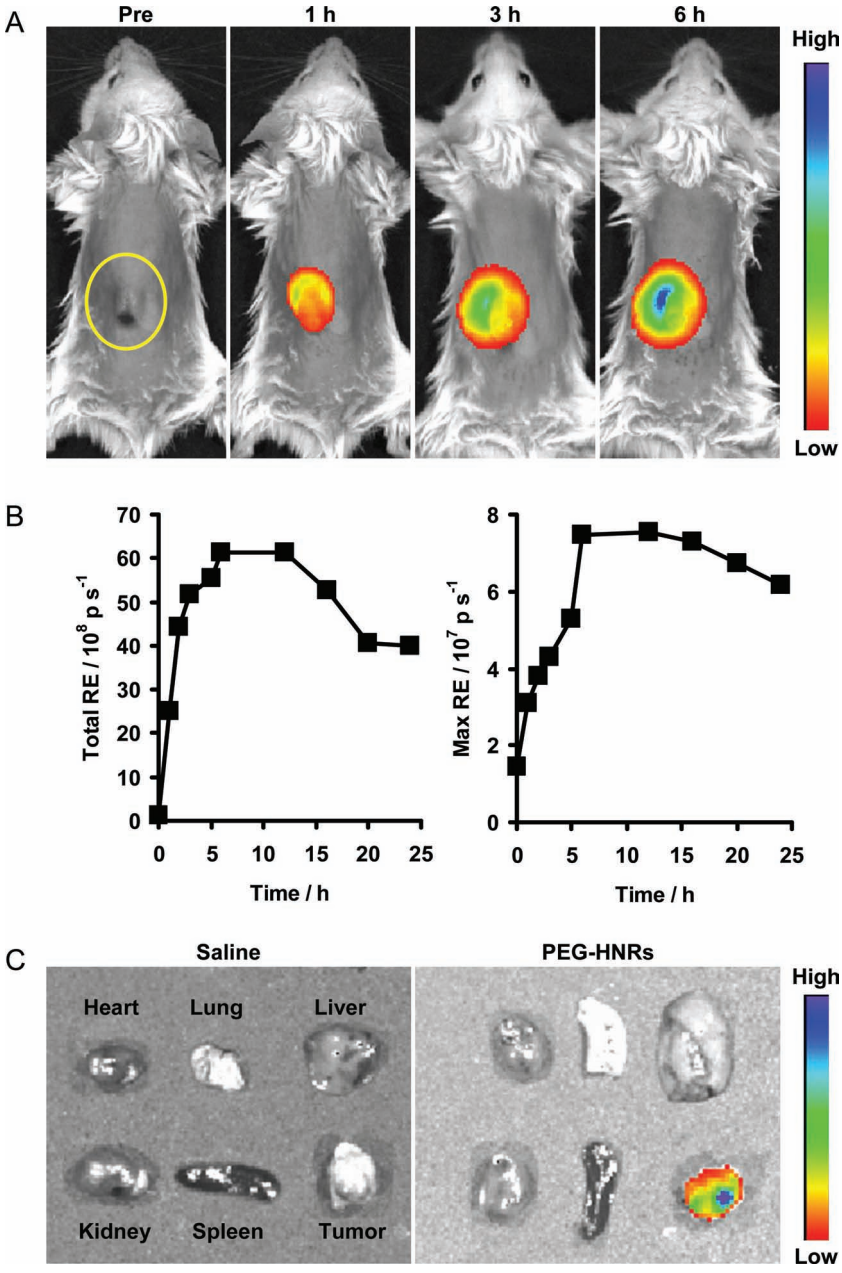

Figure 7. A) In vivo fluorescence images of tumor-bearing mouse before and after intravenous injection of PEG-HNRs at λ_{ex} = 675 nm and λ_{em} = 740 nm: preinjection, and 1, 3 and 6 h postinjection (from left to right). B) Temporal changes in total RE (left) and max RE (right) of the tumor area. C) Ex vivo fluorescence images of tissues at 6 h after injection of saline (left) and PEG-HNRs (right).

3. Conclusions

The silica/TCPP HNRs were successfully synthesized by means of the one-pot sol-gel method using TCPP-binding silica precursors. The HNRs were ring-shaped particles with a diameter of 56 nm ± 9 nm, whereas the physically synthesized TCPP-containing silica NSs were solid spherical particles with a diameter of about 243 nm. The siloxane network of HNRs consisted of Q^4, Q^3, T^3 and T^2 units and incorporated TCPP via an amide linkage. The HNRs were also functionalized with amino groups, which were useful for PEGylation. The HNRs had a significantly higher TCPP content than the NSs. Therefore, the HNRs were excited to emit strong fluorescence in the NIR region, although the NSs emitted no fluorescence. Moreover, the PEG-HNRs accumulated in tumor and could be used to clearly detect the tumor.

4. Experimental Section

Materials: TCPP, TEOS, APTES, 1-(3-dimethyl aminopropyl)-3-ethylcarbodiimide hydrochloride (EDAC), N-hydroxysuccinimide (NHS) and N,N-dimethylformamide (DMF) were purchased from Tokyo Chemical Industry (Tokyo, Japan). NHS-PEG (2 kDa) was purchased from NOF Corporation (Tokyo, Japan). Ammonia water (28%) was purchased from Kishida Chemical (Osaka, Japan).

Cell Line: Human myeloma cell line, RPMI 8226, was obtained from the Japanese Cancer Research Resources Bank (Tokyo, Japan). The cells were cultured in RPMI 1640 medium supplemented with 10% fetal bovine serum, 100 U/mL penicillin and 100 µg/mL streptomycin. Before inoculation into mice, cells were washed and resuspended in sterile phosphate-buffered saline (PBS) at a concentration of 1×10^8 cells/mL.

Animals: Female CB17/Icr-*Prkdc*^{scid} mice aged 4 weeks were purchased from Charles River Laboratories Inc. (Yokohama, Japan) and were maintained in a specific pathogen-free facility in our Animal Resources Center. All experiments were approved by the Committee on Animals of the University of Tokushima. To eradicate residual natural killer (NK) cells, mice were injected intraperitoneally with 10 µL of rabbit anti-asialo GM1 antiserum (Wako Chemicals, Osaka, Japan) at 1 day before tumor inoculation. The human myeloma cell (5×10^6 cells) inoculation was accomplished by subcutaneous injection into the backs of mice.

Characterization: The FTIR spectra were recorded with a FTIR spectrometer (Nicolet, Nexus 470, Madison, WI, USA). Solid-state ^{13}C- and ^{29}Si- CP/MAS NMR spectra of the HNRs were recorded with an Avance 300 spectrometer (Bruker BioSpin, Ettlingen, Germany) at 75.477 MHz and 59.624 MHz, respectively. The spinning rate of samples was set to 5.0 kHz. The external standards for the ^{13}C- and ^{29}Si- chemical shift were glycine and hexamethylcyclotrisiloxane, respectively. Thermal behavior of the HNRs, the NSs and the PEG-HNRs were analyzed using TG (Rigaku, TG8120, Tokyo, Japan) at a heating rate of 10 °C/min from room temperature to 800 °C under oxygen atmosphere. The morphology and size of the HNRs and the NSs were studied using TEM (Hitachi, H-760, Tokyo, Japan). The absorption bands of the HNRs and the NSs were measured using ultraviolet-visible spectrophotometer (Hitachi, U-3000, Tokyo, Japan). The hydrodynamic diameter and the zeta potential of the HNRs and the PEG-HNRs were measured by DLS (Showa Denko, NICOMP 380 ZLS, Tokyo, Japan). The fluorescence images of the HNRs- or the NSs dispersed in saline, and tumor-bearing mice injected with the PEG-HNRs, were obtained using the IVIS 200 Imaging System (Caliper Life Sciences, Hopkinton,

MA, USA). The RE value was estimated using the ROI tool, which can determine the flux (photons per second) of the target signal and compare it to the background signal. The data on blood circulation time were generated by selecting six 2 mm × 2 mm ROI per mouse, where these ROI were selected to accord with conspicuous surface blood vessels, and by tracking them through time. Mean RE values from six ROI on each mouse were measured and plotted versus time after injection.

Synthesis of Silica/TCPP HNRs: At first, TCPP-binding silica precursor was prepared as follows. APTES (15 mM) and TCPP (3.75 mM) were dissolved in DMF. EDAC (15 mM) and NHS (15 mM) were added to this solution. The mixture was stirred for 24 h at room temperature to form TCPP-binding silica precursors *via* the amidation reaction between the amino group of APTES and the carboxylic acid groups of TCPP. Next, APTES (25 mM) and TEOS (25 mM) were dissolved in the as-prepared TCPP-binding silica precursor solution and then ammonia water (2 mL) was added to this solution. The mixture was stirred for 24 h at 40 °C to yield silica/TCPP HNRs *via* the sol-gel reaction of precursors.

Synthesis of Physically Manufactured TCPP-Containing Silica NSs: TCPP (3.75 mM), TEOS (25 mM) and APTES (40 mM) were dissolved in DMF. Ammonia water (2 mL) was added to this solution. The mixture was stirred for 24 h at 40 °C to produce the physically synthesized TCPP-containing silica NSs.

PEGylation of Silica/TCPP HNRs: NHS-PEG (10 μmol) was added to the HNRs-dispersed water (4 mg/mL). This suspension was stirred for 24 h at 25 °C to yield PEG-HNRs *via* the amidation reaction between the amino groups of the HNRs and the NHS active ester groups of NHS-PEG.

Supporting Information

Supporting Information is available from the Wiley Online Library or from the author.

Acknowledgements

This work was supported in part by Grant-in-Aid for Young Scientists (B) (24760551) from the Ministry of Education, Science, Sports, and Culture of Japan.

Received: January 24, 2012
Revised: March 30, 2012
Published online: May 10, 2012

[1] C. Sun, J. Yang, L. Li, X. Wu, Y. Liu, S. Liu, *J. Chromatogr. A* **2004**, *803*, 173.
[2] K. Stefflova, J. Chen, G. Zheng, *Front. Biosci.* **2007**, *12*, 4709.
[3] P. P. Ghoroghchian, M. J. Therien, D. A. Hammer, *Wiley Interdiscip. Rev. Nanomed. Nanobiotechnol.* **2009**, *1*, 156.
[4] X. He, K. Wang, Z. Cheng, *Wiley Interdiscip. Rev. Nanomed. Nanobiotechnol.* **2010**, *2*, 349.
[5] R. A. Weissleder, *Nat. Biotechnol.* **2001**, *19*, 316.
[6] M. Velusamy, J.-Y. Shen, J. T. Lin, Y.-C. Lin, C.-C. Hsieh, C.-H. Lai, C.-W. Lai, M.-L. Ho, Y.-C. Chen, P.-T. Chou, J.-K. Hsiao, *Adv. Funct. Mater.* **2009**, *19*, 2388.
[7] F. Würthner, T. E. Kaiser, C. R. Saha-Möller, *Angew. Chem. Int. Ed.* **2011**, *50*, 3376.
[8] Z. Wang, C. J. Medforth, J. A. Shelnutt, *J. Am. Chem. Soc.* **2004**, *126*, 15954.
[9] S. Sadasivan, K. Köhler, G. B. Sukhorukov, *Adv. Funct. Mater.* **2006**, *16*, 2083.
[10] K. Hayashi, M. Nakamura, K. Ishimura, *Chem. Commun.* **2012**, *48*, 3830.
[11] H. Maeda, J. Wu, T. Sawa, Y. Matsumura, K. Hori, *J. Controlled Release* **2000**, *65*, 271.
[12] S. C. Doan, S. Shanmugham, D. E. Aston, J. L. McHale, *J. Am. Chem. Soc.* **2005**, *127*, 5885.
[13] P. Couleaud, V. Morosini, Céline Frochot, S. Richeter, L. Raehma, J.-O. Durand, *Nanoscale* **2010**, *2*, 1083.
[14] H.-L. Tu, Y.-S. Lin, H.-Y. Lin, Y. Hung, L.-W. Lo, Y.-F. Chen, C.-Y. Mou, *Adv. Mater.* **2009**, *21*, 172.
[15] S.-H. Cheng, C.-H. Lee, C.-S. Yang, F.-G. Tseng, C.-Y. Moud, L.-W. Lo, *J. Mater. Chem.* **2009**, *19*, 1252.
[16] S.-H. Cheng, C.-H. Lee, M.-C. Chen, J. S. Souris, F.-G. Tseng, C.-S. Yang, C.-Y. Mou, C.-T. Chend, L.-W. Lo, *J. Mater. Chem.* **2010**, *20*, 6149.
[17] T. Y. Ohulchanskyy, I. Roy, L. N. Goswami, Y. Chen, E. J. Bergey, R. K. Pandey, A. R. Oseroff, P. N. Prasad, *Nano Lett.* **2007**, *7*, 2835.
[18] L. M. Rossi, P. R. Silva, L. L. R. Vono, A. U. Fernandes, D. B. Tada, M. S. Baptista, *Langmuir* **2008**, *24*, 12534.
[19] D. Brevet, M. Gary-Bobo, L. Raehm, S. Richeter, O. Hocine, K. Amro, B. Loock, P. Couleaud, C. Frochot, A. Morère, P. Maillard, M. Garcia, J.-O. Durand, *Chem. Commun.* **2009**, 1475.
[20] K. Hayashi, M. Nakamura, K. Ishimura, *Chem. Commun.* **2011**, *47*, 1518.
[21] H. J. Hah, J. S. Kim, B. J. Jeon, S. M. Koo, Y. E. Lee, *Chem. Commun.* **2003**, 1712.
[22] Q. Wang, Y. Liu, H. Yan, *Chem. Commun.* **2007**, 2339.
[23] J. M. Harris, R. B. Chess, *Nat. Rev. Drug Discovery* **2003**, *2*, 214.
[24] N. Primeau, C. Vautey, M. Langlet, *Thin Solid Films.* **1997**, *47*, 310.
[25] A. S. M. Chong, X. S. Zhao, *J. Phys. Chem. B* **2003**, *107*, 12650.
[26] Z. Zhang, A. L. Verma, M. Yoneyama, K. Nakashima, K. Iriyama, Y. Ozaki, *Langmuir* **1997**, *13*, 4422.
[27] A. Fidalgo, L. M. Ilharco, *J. Non-Cryst. Solids.* **2001**, *283*, 144.
[28] Y. Gao, N. R. Choudhury, N. Dutta, J. Matisons, M. Reading, L. Delmotte, *Chem. Mater.* **2001**, *13*, 3644.
[29] R. Rahimi, F. Moharrami, S. H. Rahmanpor, *Asian J. Chem.* **2010**, *22*, 4398.
[30] R. M. Silverstein, F. X. Webster, D. J. Kiemle, *Spectrometric Identification of Organic Compounds*, 7th Ed., John Wiley & Sons, New York **2005**.
[31] T. Maldiney, C. Richard, J. Seguin, N. Wattier, M. Bessodes, D. Scherman, *ACS Nano* **2011**, *5*, 854.
[32] G. Urbinati, D. Audisio, V. Marsaud, V. Plassat, S. Arpicco, B. Sola, E. Fattal, J.-M. Renoir, *Pharmacol. Res.* **2010**, *27*, 327.
[33] S. Maillard, J. Gauduchon, V. Marsaud, F. Gouilleux, E. Connault, P. Opolon, E. Fattal, B. Sola, J.-M. Renoir, *J. Steroid Biochem. Mol. Biol.* **2006**, *100*, 67.
[34] S. Maillard, T. Ameller, J. Gauduchon, A. Gougelet, F. Gouilleux, P. Legrand, V. Marsaud, E. Fattal, B. Sola, J.-M. Renoir, *J. Steroid Biochem. Mol. Biol.* **2005**, *94*, 111.
[35] S. Mitragotri, J. Lahann, *Nat. Mater.* **2009**, *8*, 15.
[36] N. Doshi, S. Mitragotri, *Adv. Funct. Mater.* **2009**, *19*, 3843.
[37] N. Doshi, S. Mitragotri, *PloS One* **2010**, *5*, e10051.
[38] J. A. Champion, Y. K. Katare, S. Mitragotri, *J. Controlled Release* **2007**, *121*, 3.
[39] J. A. Champion, S. Mitragotri, *Pharm. Res.* **2009**, *26*, 244.
[40] J. A. Champion, S. Mitragotri, *Proc. Natl. Acad. Sci. USA* **2006**, *103*, 4930.
[41] X. He, H. Nie, K. Wang, W. Tan, X. Wu, P. Zhang, *Anal. Chem.* **2008**, *80*, 9597.